Prototype Charts for Identifying Biaxial Phases

Ludo K. Frevel

Department of Chemistry, The Johns Hopkins University, Baltimore Md. 21218

The procedure for the systematic identification of uniaxial isomorphs has been extended to biaxial isomorphs. Novel prototype charts for the orthorhombic, monoclinic, and triclinic system are presented to illustrate a convenient graphical method of indexing powder patterns of biaxial phases.

GENERAL PROCEDURES for comparing powder diffraction patterns of isomorphous substances have been published for uniaxial crystals (*1–3*). To extend this systematic identification of crystalline phases to biaxial crystals necessitates an effective modification of the familiar semilogarithmic chart of interplanar distance *vs.* relative intensity. For uniaxial structures one parameter, namely the axial ratio c/a, suffices to describe a set of isomorphous powder patterns. For the simplest biaxial crystals at least two axial ratios (a/b and c/b) are required to cover the variations in the interplanar spacings for different compounds of an isomorphous series. The three biaxial systems (orthorhombic, monoclinic, and triclinic) are treated separately below and prototype charts are included to assist the diffractionist in identifying an unknown powder pattern and in indexing the first 10 to 20 *d*-spacings of a matched phase.

ORTHORHOMBIC ISOMORPHS

To circumvent the awkwardness of three-dimensional curves depicting the first 20 interplanar spacings of a set of orthorhombic isomorphs, a series of log d_{hkl} strips has been developed by imposing systematic constraints on the three lattice constants (a, b, c) or on the two axial ratios (a/b or c/b) in order to follow graphically the effect of a single parameter on the resultant powder patterns.

The principle by which the charts are constructed can be illustrated with the barite structure. The arithmetic mean of the respective lattice constants of the 25 known isomorphs of $BaSO_4$ (see Table I) are $\bar{a}$ = 7.228 Å (6.613 Å to 7.813 Å), $\bar{b}$ = 8.917 Å (8.307 Å to 9.848 Å), and $\bar{c}$ = 5.635 Å (5.291 Å to 6.07 Å). Imposing the first constraint that the axial ratio $a/b = r_1$ be held constant, one can plot log d_{hkl} as a function of $c/b = r_2$ according to Equation 1.

$$\log d_{hkl} + \text{constant} = -\tfrac{1}{2} \log (h^2 r_1^{-2} + k^2 + l^2 r_2^{-2}) \quad (1)$$

A judicious selection for r_1 is the arithmetic mean of a/b; namely, 0.8110 which is very close to $\bar{a}/\bar{b}$ = 0.8106. However, it is not essential to select precisely either value; any value close to the most probable value of a/b is equally suitable for constructing the curves for d_{hkl} (r_2) depicted in Figure 1 for the case where a and b are held constant. The parameter r_2 in Equation 1 is varied over the narrow ranges 0.600 to 0.630 and 0.630 to 0.660 to facilitate the unique indexing of interplanar spacings. It is obvious that the $hk0$ reflections fall on vertical lines for the top split strip of Figure 1. The relative intensities depicted in the middle of the split strip pertain to $SrSO_4$ although the log d_{hkl} values are not exactly those for pure $SrSO_4$ (r_2 = 0.6403). The second split strip with b and c constant and the third strip with a and c constant are constructed in an analogous fashion.

When only one lattice parameter is held constant, for example b, then log d_{hkl} can be plotted as a function of paired values of r_1 and r_2. The appropriate pairing of r_1 and r_2 within their known ranges ($0.7575 \leqslant r_1 \leqslant 0.8585$ and $0.5983 \leqslant r_2 \leqslant 0.6919$) is guided by the data of Table I. To keep the strips uniformly narrow, the upper limits of r_1 and r_2 were trimmed somewhat without much loss of utility. The family of six split strips in Figure 1 also gives information on changes in relative intensities with changes in M^{n+} and $(RX_4)^{n-}$.

The following example illustrates the application of the orthorhombic charts in identifying an unknown phase. Columns 2 and 3 of Table II give the diffraction data of a white precipitate exposed to $CuK\alpha_1$ radiation in an AEG double cylinder Guinier camera (114.7-mm diam) at Dow's Chemical Physics Research Laboratory. Starting with the strongest line (2.974 Å) and searching in the ASTM Powder Diffraction File (*4*), one readily matches 11 spacings of $SrSO_4$. On closer inspection the approximate match suggests a slightly expanded celestite structure. Calculation of the lattice constants by the axial ratios method (*5*) yields a = 6.876 Å, b = 8.373 Å, and c = 5.357 Å. For the remaining 14 lines, no convincing match is found in the files of published standards. Noting, however, that the strongest lines of the $SrSO_4$ pattern are paired with the strongest lines of the residual pattern (d_{13} and d_{14}, d_9 and d_{10}, d_{11} and d_{12}, d_{15} and d_{16}, d_4 and d_5), one surmises that the unidentified phase may be isomorphous with $SrSO_4$. To validate this guess, one indexes the unknown pattern with the aid of the orthorhombic charts of Figure 1. One plots log d of the 14 residual lines and their corresponding relative intensities (downward bars) on a narrow strip of paper and then attempts to match the intense lines in any of the six strips. Starting with the top strip, one gets an immediate match with the strongest lines of the $SrSO_4$ pattern at $c/b \approx 0.635$ and unique indexing of 9 reflections (111, 120, 200, 021, 210, 121, 211, 130, 022). The second strip gives a better match with the relative intensities and a good match at $a/b \approx 0.820$ and unique indexing for the same 9 reflections. The fourth strip gives a good match at $a/b \approx 0.815$ and $c/b \approx 0.635$ with unique indexing for 10 reflections (111, 120, 200, 021, 210, 121, 211, 130, 022, 230). However, the relative intensity of the first unresolved reflection (101, 020) is too high. Computing the lattice constants from the indexed reflections (*5*), one obtains a = 6.976 Å, b = 8.558 Å, c = 5.411 Å. X-ray fluorescence data reveal Sr, Ba, and S as the major elements. Accordingly one can combine the structural information with the elemental data and write the composition of the two solid solution phases as $Sr_{1-x}Ba_xSO_4$ and $Ba_{1-y}Sr_ySO_4$. From the expansion of the celestite structure and the contraction of the barite structure, one can compute (*6*) the value of x = 0.037 and of y = 0.435. The calculated intensities in Table II are not corrected for the substitution of

(1) L. K. Frevel, IND. ENG. CHEM., ANAL. ED., **14,** 687 (1942).
(2) *Ibid.*, **18,** 83 (1946).
(3) L. K. Frevel and H. W. Rinn, ANAL. CHEM., **25,** 1697 (1953).
(4) "Index (Inorganic) to the Powder Diffraction File 1971," Joint Committee on Powder Diffraction Standards, 1601 Park Lane, Swathmore, Pa. 19081.
(5) L. K. Frevel, *Acta Crystallogr.*, **17,** 907 (1964).
(6) L. K. Frevel, ANAL. CHEM., **42,** 1583 (1970).

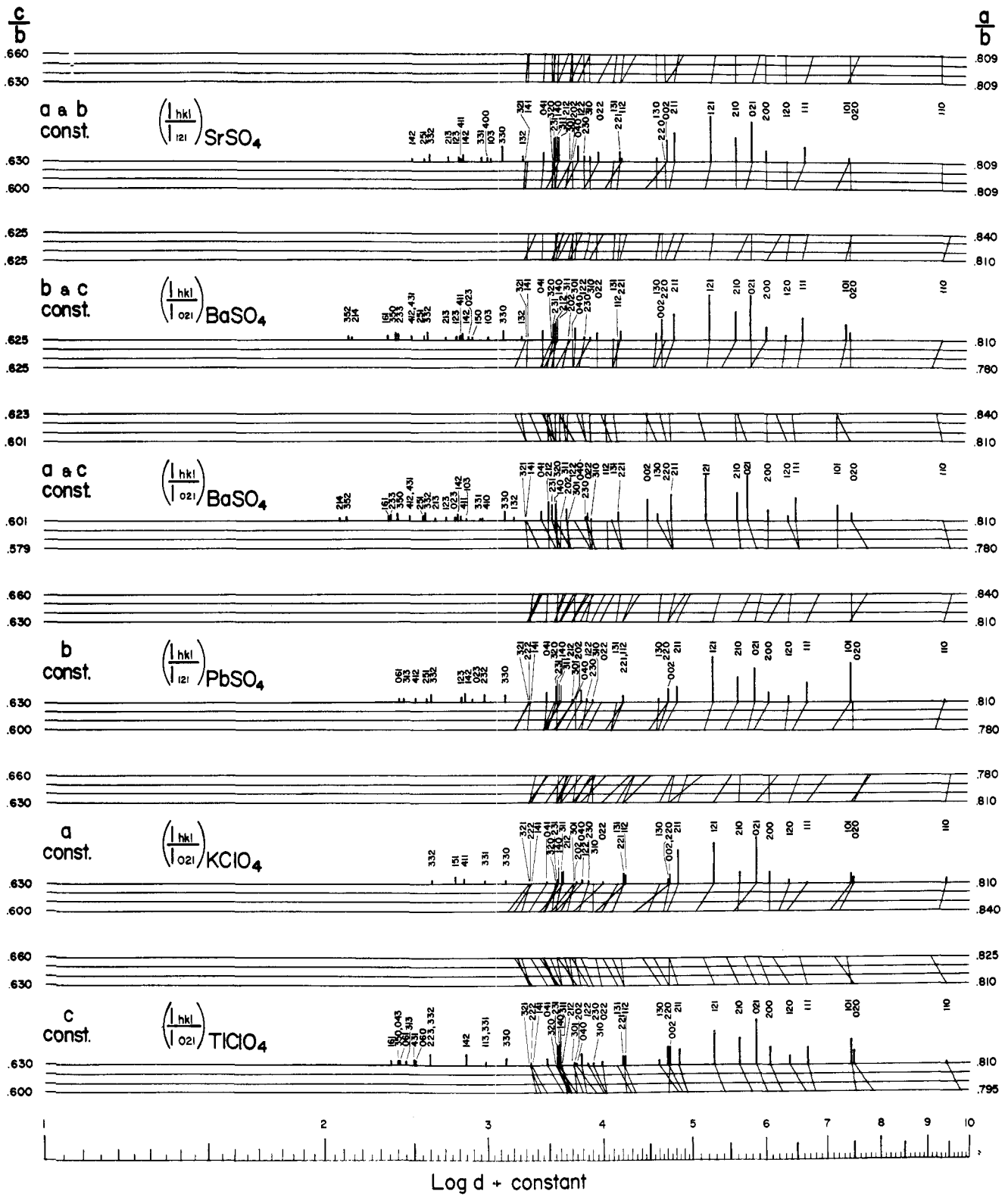

Figure 1. Representative powder diffraction patterns for the orthorhombic isomorphs of barite

Ba for Sr in $SrSO_4$ and the substitution of Sr for Ba in $BaSO_4$ (*7*).

The utility of the orthorhombic charts of Figure 1 is not limited to identifying the barite structure but can also be used to index orthorhombic phases with axial ratios falling within 0.600 and 0.840. Having indexed an unknown pattern and calculated the lattice constants, one can then search under the axial ratio index in the "Crystal Data Determinative Tables" (*8*) for a likely orthorhombic candidate.

(7) L. K. Frevel, ANAL. CHEM., **40**, 1335 (1968).

MONOCLINIC ISOMORPHS

Charts for monoclinic isomorphs are developed in the following manner. For a particular structure such as $H4_4$ exemplified by the 37 known Tutton salts (see Table III), the average lattice constants are $\bar{a}$ = 9.276 Å, $\bar{b}$ = 12.557 Å, $\bar{c}$ =

Table I. Cell Data for $M^{n+}(RX_4)^{n-}$ with Barite Structure

V[a], Å^3	a/b	c/b	a, Å	b, Å	c, Å	Formula	Reference
298.3	0.8170	0.6369	6.787	8.307	5.291	β-$SrBeF_4$	(*8*) O–0.8170
307.2	0.8214	0.6403	6.866	8.359	5.352	$SrSO_4$	(*9*)
309.7	0.8151	0.6332	6.875	8.435	5.341	$PbBeF_4$	(*9*)
313.5	0.8156	0.6348	6.90	8.46	5.37	$EuSO_4$	(*8*) O–0.8156
318.5	0.8205	0.6366	6.958	8·480	5.398	$PbSO_4$	(*9*)
326.2	0.7575	0.6472	6.613	8.73	5.65	$BaBeF_4$	(*9*)
340.1	0.8155	0.6162	7.16	8·78	5.41	$BaBOF_3$	(*9*)
344.9	0.8297	0.6553	7.129	8.592	5.63	β-$PbSeO_4$	(*9*)
346.0	0.8058	0.6144	7.151	8.874	5.452	$BaSO_4$	
353.1	0.7836	0.6369	6.983	8.911	5.675	$NOBF_4$	(*10*)
355.8	0.8387	0.6486	7.28	8.68	5.63	$BaPO_3F$	(*9*)
361.9	0.8020	0.5983	7.301	9.103	5.446	$BaFeO_4$	(*9*)
363.8	0.8190	0.6394	7.254	8.857	5.663	$KClO_4$	(*9*)
364.1	0.8057	0.6039	7.315	9.079	5.483	$BaMnO_4$	(*9, 11*)
369.6	0.8033	0.6311	7.23	9.00	5.68	$(NO)ClO_4$	(*9*)
370.9	0.8049	0.6068	7.343	9.123	5.536	$BaCrO_4$	(*9, 11*)
374·0	0.8588	0.6919	7.36	8.57	5.93	KSO_3F	(*9*)
377.7	0.8155	0.6280	7.368	9.035	5.674	β-$BaSeO_4$	(*9, 11*)
390.6	0.8328	0.6906	7.32	8.79	6.07	NH_4SO_3F	(*9*)
403.6	0.8081	0.6273	7.490	9.269	5.814	$RbClO_4$	(*9*)
407.2	0.7814	0.6135	7.40	9.47	5.81	$TlBF_4$	(*9*)
408.4	0.8072	0.6282	7.510	9.304	5.845	$TlClO_4$	(*9*)
409.7	0.8328	0.6298	7.67	9.21	5.80	$RbSO_3F$	(*9*)
434.7	0.7906	0.6104	7.636	9.658	5.895	$CsBF_4$	(*9*)
463.9	0.7934	0.6122	7.813	9.848	6.029	$CsClO_4$	(*12*)

[a] Isomorphs arranged in ascending order of V, volume of unit cell.

Table II. X-Ray Powder Diffraction Data of Precipitate

Precipitate			Phase I[a]			Phase II		
ν	d_ν, Å	I_ν	hkl	d_{calcd}, Å	I_{calcd}	hkl	d_{calcd}, Å	I_{calcd}
						020	4.2790	5.0
1	4.276	9.8				101	4.2755	10.8
2	4.226	5.0	101	4.2257	4.5			
3	4.190	2.7	020	4.1863	3.3			
4	3.825	16.3				111	3.8248	15.6
5	3.776	14.8	111	3.7725	14.5			
6	3.654	1.8				120	3.6474	3.5
7	3.490	7.2				200	3.4880	7.9
			120	3.5758	0.8			
8	3.438	13.6	200	3.4382	12.4			
9	3.353	38.5				021	3.3563	29.3
10	3.2985	46.7	021	3.2984	40.7			
11	3.2298	16.8				210	3.2300	19.4
12	3.1816	28.9	210	3.1804	24.5			
13	3.0235	36.7				121	3.0244	28.7
14	2.9740	47.6	121	2.9740	41.5			
15	2.7706	5.4				211	2.7734	13.8
16	2.7372	20.8	211	2.7347	26.1			
						002	2.7055	12.9
17	2.7074	15.7				220	2.7035	<0.2
18	2.6783	14.2	002	2.6783	20.3			
19	2.6442	1.7				130	2.6404	4.7
20	2.5893	1.8	130	2.5860	2.5			
						112	2.4195	<0.2
21	2.4205	3.5				221	2.4185	3.8
			112	2.3916	2.9			
22	2.3833	4.4	221	2.3802	7.1			
23	2.2847	3.5				022	2.2867	3.8
24	2.2077	2.9				230	2.2081	1.8
25	2.1719	7.8				122	2.1729	6.5

[a] Phase I is $Sr_{0.963}Ba_{0.037}SO_4$; Phase II, $Ba_{0.565}Sr_{0.435}SO_4$.

(8) J. D. H. Donnay, G. Donnay, E. G. Cox, O. Kennard, and M. V. King, "Crystal Data Determinative Tables," 2nd ed., American Crystallographic Association, Williams and Heintz Map Corporation, 8351 Central Ave., Washington 27, D.C., 1963.
(9) R. W. G. Wyckoff, "Crystal Structures," 2nd ed., Vol. 3, Interscience, New York, N.Y., 1965, pp 45–51.
(10) J. C. Evans, H. W. Rinn, S. J. Kuhn, and G. A. Olah, *Inorg. Chem.*, **3**, 857 (1964).
(11) L. K. Frevel, *J. Appl. Phys.*, **13**, 109 (1942).
(12) H. E. Swanson, M. C. Morris, R. P. Stinchfield, and E. H. Evans, *Nat. Bur. Stand. (U.S.) Monogr.*, **25**, Section 1, 10 (1962).

6.253 Å, and $\bar{\beta} = 106.2°$. Holding any three lattice parameters constant at or near their respective arithmetic mean, one can plot log d_{hkl} as a function of the nonconstrained parameter. For example the angle β for the known Tutton salts varies from 104.8° to 107.2°. In the top strip of Figure 2, β is varied from 104° to 110° whereas the cell edges are held constant at their most probable values so that $a/b = r_1 = 0.738$ and $c/b = r_2 = 0.496$. The change of log d_{hkl} as a function of β is given by Expression 2.

Table III. Cell Data for $M_2^{+}M^{2+}(OH_2)_6(XR_4)_2^{2-}$ with $H4_4$ Structure

V, Å^3	a/b	c/b	a, Å	b, Å	c, Å	β, °	Formula	Reference
647.41	0.7344	0.4907	9.06	12.33	6.05	106.68	$(NH_4)_2Ni(BeF_4)_2\cdot 6H_2O$	(*13*)
648.90	0.7382	0.5032	8.994	12.184	6.131	105.02	$K_2Ni(SO_4)_2\cdot 6H_2O$	
657.24	0.7402	0.5040	9.041	12.215	6.156	104.82	$K_2Zn(SO_4)_2\cdot 6H_2O$	(*14*)
657.78	0.7423	0.5039	9.061	12.207	6.151	104.80	$K_2Co(SO_4)_2\cdot 6H_2O$	(*15*)
660.44	0.7423	0.5001	9.096	12.254	6.128	104.78	$K_2Mg(SO_4)_2\cdot 6H_2O$	(*16*)
677.55	0.7397	0.5016	9.166	12.392	6.216	106.33	$Tl_2Ni(SO_4)_2\cdot 6H_2O$	(*14*)
678.48	0.7360	0.5012	9.138	12.416	6.223	106.06	$Rb_2Ni(SO_4)_2\cdot 6H_2O$	(*16*)
683.46	0.7384	0.5011	9.180	12.433	6.230	106.02	$Rb_2Co(SO_4)_2\cdot 6H_2O$	(*15*)
685.59	0.7415	0.5012	9.219	12.433	6.232	106.29	$Tl_2Zn(SO_4)_2\cdot 6H_2O$	(*14*)
686.20	0.7496	0.5027	9.268	12.364	6.216	105.56	$Tl_2Cu(SO_4)_2\cdot 6H_2O$	(*14*)
686.38	0.7422	0.5005	9.235	12.442	6.227	106.40	$Tl_2Co(SO_4)_2\cdot 6H_2O$	(*14*)
686.45	0.7378	0.5014	9.185	12.450	6.242	105.91	$Rb_2Zn(SO_4)_2\cdot 6H_2O$	(*14*)
687.43	0.7368	0.4993	9.211	12.502	6.241	106.96	$(NH_4)_2Ni(SO_4)_2\cdot 6H_2O$	(*13*, *17*)
688.35	0.7494	0.5036	9.267	12.366	6.228	105.32	$Rb_2Cu(SO_4)_2\cdot 6H_2O$	(*16*)
689.49	0.7435	0.4982	9.273	12.472	6.214	106.38	$Tl_2Mg(SO_4)_2\cdot 6H_2O$	(*14*)
689.93	0.7396	0.4985	9.235	12.486	6.224	105.98	$Rb_2Mg(SO_4)_2\cdot 6H_2O$	(*16*)
690.58	0.7386	0.4984	9.247	12.519	6.239	107.03	$(NH_4)_2Co(SO_4)_2\cdot 6H_2O$	(*15*)
693.58	0.7412	0.4989	9.264	12.499	6.236	106.15	$Tl_2Fe(SO_4)_2\cdot 6H_2O$	(*16*)
693.62	0.7376	0.5006	9.218	12.497	6.256	105.75	$Rb_2Fe(SO_4)_2\cdot 6H_2O$	(*16*)
697.67	0.7446	0.5061	9.267	12.445	6.298	106.15	$(NH_4)_2Cu(SO_4)_2\cdot 6H_2O$	(*18*)
698.02	0.7383	0.4975	9.279	12.568	6.253	106.82	$(NH_4)_2Zn(SO_4)_2\cdot 6H_2O$	(*13*)
698.76	0.7383	0.4948	9.30	12.60	6.23	106.83	$(NH_4)_2Fe(SO_4)_2\cdot 6H_2O$	(*13*)
702.03	0.7404	0.4920	9.354	12.633	6.216	107.11	$(NH_4)_2Mg(SO_4)_2\cdot 6H_2O$	(*13*, *17*)
711.22	0.7395	0.4933	9.374	12.676	6.253	106.82	$(NH_4)_2Mn(SO_4)_2\cdot 6H_2O$	(*16*)
716.47	0.7474	0.4979	9.420	12.603	6.275	105.90	$(NH_4)_2Ni(CrO_4)_2\cdot 6H_2O$	(*16*)
719.64	0.7253	0.4978	9.264	12.773	6.359	106.98	$Cs_2Ni(SO_4)_2\cdot 6H_2O$	(*14*)
719.86	0.7536	0.4977	9.474	12.571	6.256	104.95	$Rb_2Mg(CrO_4)_2\cdot 6H_2O$	(*16*)
722.67	0.7502	0.4928	9.508	12.674	6.246	106.23	$(NH_4)_2Mg(CrO_4)_2\cdot 6H_2O$	(*16*)
724.11	0.7354	0.4930	9.395	12.776	6.299	106.72	$(NH_4)_2Cd(SO_4)_2\cdot 6H_2O$	(*16*)
726.73	0.7265	0.4963	9.316	12.824	6.365	107.12	$Cs_2Co(SO_4)_2\cdot 6H_2O$	(*15*)
727.79	0.7270	0.4973	9.316	12.815	6.373	106.95	$Cs_2Zn(SO_4)_2\cdot 6H_2O$	(*14*)
727.81	0.7406	0.4953	9.44	12.74	6.31	106.45	$(NH_4)_2Mg(SeO_4)_2\cdot 6H_2O$	(*13*)
728.94	0.7262	0.4950	9.330	12.848	6.360	107.03	$Cs_2Mg(SO_4)_2\cdot 6H_2O$	(*14*)
729.99	0.7396	0.4994	9.439	12.762	6.310	106.18	$Cs_2Cu(SO_4)_2\cdot 6H_2O$	(*14*)
736.12	0.7256	0.4947	9.355	12.893	6.378	106.88	$Cs_2Fe(SO_4)_2\cdot 6H_2O$	(*14*)
746.56	0.7263	0.4924	9.425	12.976	6.389	107.17	$Cs_2Mn(SO_4)_2\cdot 6H_2O$	(*14*)
761.23	0.7414	0.4917	9.604	12.953	6.369	106.10	$Cs_2Mg(CrO_4)_2\cdot 6H_2O$	(*16*)

Table IV. Powder Diffraction Data of $K_2Ni(SO_4)_{2-x}(SeO_4)_x\cdot 6H_2O$[a]

d_{obsd}, Å	I_{obsd}	hkl	d_{calcd}, Å	I, (*19*)
7.137	3	110	7.120	
6.127	11	020	6.120	20
5.966	2	001	5.963	5
5.359	18	011	5.361	20
5.128	3	$\bar{1}11$	5.128	10
5.015	4	120	5.016	5
4.376	19	200	4.377	20
4.271	13	021	4.271	15
4.161	85	111	4.164	75
4.119	7	210	4.121	
4.059	70	$\bar{2}01$	4.059	75
3.852	4	$\bar{2}11$	3.853	5
3.698	100	130	3.698	100
3.587	10	121	3.587	15
3.558	3	220	3.560	
3.367	11	031	3.3672	10
3.306	16	$\bar{1}31$	3.3072	20
3.162	15	201	3.1625	15
3.060	35	211	3.0620	30
		040	3.0600	
2.9794	40	230	2.9843	55
		002	2.9813	
		$\bar{1}12$	2.9803	
2.8748	2	$\bar{2}31$	2.8777	5
2.8526	3	$\bar{3}11$	2.8537	
2.8370	4	310	2.8382	20
2.8226	3	$\bar{2}02$	2.8238	
2.8081	14	221	2.8096	15
2.7458	12B	$\bar{2}12$	2.7515	15
		$\bar{1}22$	2.7461	
		041	2.7224	
2.6890	4	$\bar{1}41$	2.6904	5
2.6435	3	$\bar{3}21$	2.6461	5

[a] a = 9.056 Å, b = 12.240 Å, c = 6.169 Å, β = 104.86° Intensities given in arbitrary units.

$$\log d_{hkl} + \text{constant} = -\tfrac{1}{2}\log[(h^2r_1^{-2} - 2hlr_1^{-1}r_2^{-1}\cos\beta + l^2r_2^{-2})\sin^{-2}\beta + k^2] \quad (2)$$

In strip 2, illustrated by $K_2Mg(SO_4)_2\cdot 6H_2O$, r_1 and β are held constant and r_2 is varied from 0.465 to 0.525, which interval is somewhat broader than that exhibited in Table III ($0.4907 < c/b < 0.5061$). In strip 3, the axial ratio r_1 ranges from 0.710 to 0.770 ($0.7253 < a/b < 0.7536$ for Table III). Since $r_2/r_1 = c/a$, no strip was constructed for the case where c/a and β are held constant. When only two lattice constants are fixed, for example a and b, then $\log d_{hkl}$ must be plotted as a function of paired values of c and β. Judicious pairing of r_2 and β within their known ranges is dictated by the data of Table III and is arranged so that the central d values of a split strip approximate those of the cited isomorph; *e.g.*, $(NH_4)_2Ni(SO_4)_2\cdot 6H_2O$ for split strip 4. Although six cases of pairing lattice constants are possible, the three cases illustrated by the

(13) R. W. Wyckoff, "Crystal Structures," 2nd ed., Vol. 3, Interscience, New York, N.Y., 1965, pp 821–824.
(14) H. E. Swanson, H. F. McMurdie, M. C. Morris, and E. H. Evans, *Nat. Bur. Stand. (U.S.) Monogr.*, **25**, Section 7, 14–80 (1969).
(15) P. Hartman and C. F. Woensdregt, *Acta Crystallogr.*, **17**, 779 (1964).
(16) H. E. Swanson, H. F. McMurdie, M. C. Morris, and E. H. Evans, *Nat. Bur. Stand. (U.S.) Monogr.*, **25**, Section 8, 5–87 (1970).
(17) H. Montgomery and E. C. Lingafelter, *Acta Crystallogr.*, **17**, 1478 (1964).
(18) *Ibid.*, **20**, 659 (1966).
(19) J. E. Weidenborner, I. Tsu, and L. E. Godycki, *ibid.*, **14**, 63 (1961).

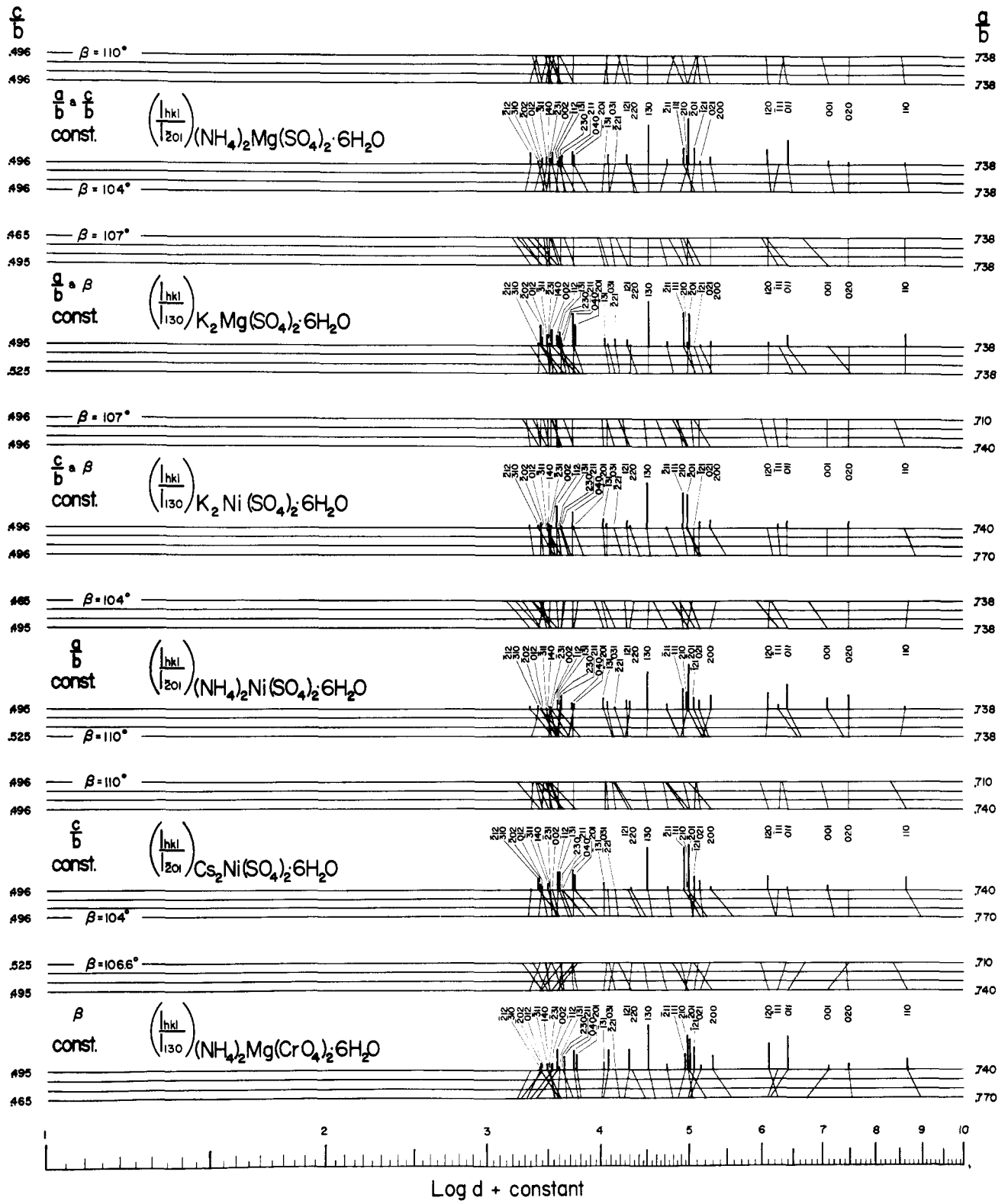

Figure 2. Representative powder diffraction patterns for the monoclinic Tutton salts

split strips 4 to 6 are adequate for identifying the $H4_4$ structure. As in the case of the orthorhombic charts, the family of six split strips in Figure 2 gives pertinent information on changes in relative intensities for various combinations of cations in Tutton salts. The relative intensities for Figures 1 and 2 are based on NBS data (*14*, *16*) and Dow data.

An attempt was made to cocrystallize K_2SO_4, K_2SeO_4, and 2 $Ni(SO_4)\cdot 7H_2O$ from a concentrated aqueous solution to obtain $K_2Ni(SO_4)(SeO_4)\cdot 6H_2O$. The resultant crystals were examined by precision powder diffraction with $CuK\alpha_1$ radiation. Columns 1 and 2 of Table IV reproduce the first 28 *d* spacings and their corresponding intensities. To confirm that the cocrystallized material is a single phase with the $H4_4$ structure, one attempts to index the pattern with the aid of the *monoclinic charts of* Figure 2. Using the logarithmic scale at the base of Figure 2, one plots log *d* and the corresponding

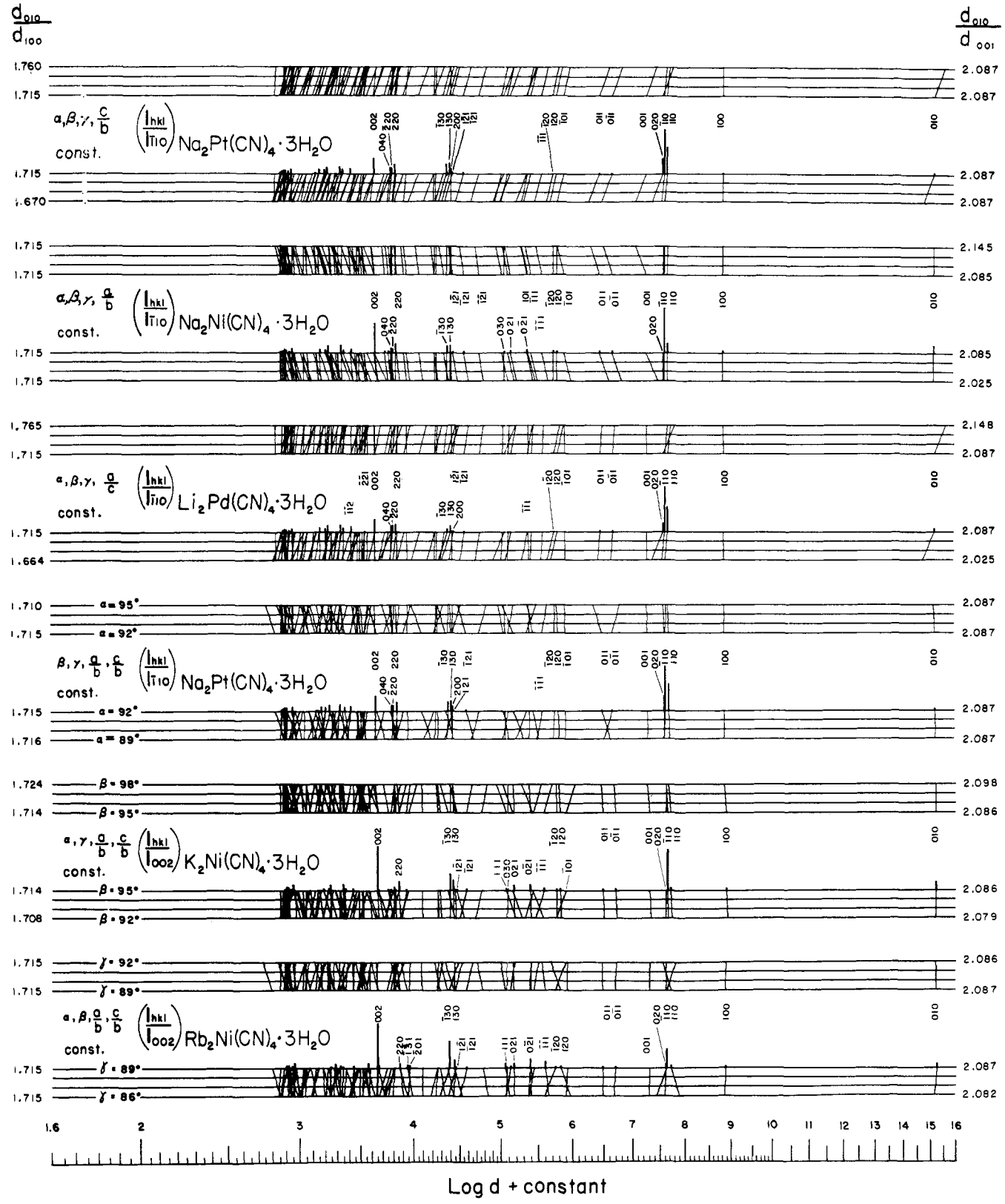

Figure 3. Representative powder diffraction patterns for the triclinic isomorphs of $Na_2Ni(CN)_4\cdot 3H_2O$

relative intensity on a narrow strip of paper and then proceeds to match the intense lines and the *innermost* lines. Starting with the top strip and attempting to index the first reflection, one gets a fairly good match for $\beta = 105°$ and unique indexing for 110, 020, 001, 011, $\bar{1}11$, 120, 200, 021, $\bar{2}11$, and 130. The intensity match, however, is relatively poor. For strip 3, a good intensity match is noted, especially for 111 and $\bar{2}01$. The $hk0$ reflections match well on strip 1 at $\beta = 105°$, $a/b = 0.738$, and $c/b = 0.496$; the $0kl$ reflections match well with $c/b \approx 0.50$ on strips 4 and 6. Using the axial ratios method (*10*), one computes the lattice constants $a = 9.056 \pm 0.002$ Å, $b = 12.240 \pm 0.003$ Å, $c = 6.169 \pm 0.001$ Å, and $\beta = 104.86° \pm 0.05°$. The calculated d spacings of Table IV are based on this unit cell and the corresponding relative intensities are

Table V. Cell Data[a] for Isomorphs of $Na_2Ni(CN)_4 \cdot 3H_2O$

V, Å^3	a, Å	b, Å	c, Å	α, °	β, °	γ, °	Formula
956.49	8.84	15.01	7.25	92.38	95.60	89.05	$Li_2Ni(CN)_4 \cdot 3H_2O$
958.04	8.80	15.10	7.25	92.62	95.38	88.98	$(NH_4)_2Ni(CN)_4 \cdot 3H_2O$
969.25	8.84	15.01	7.34	92.27	95.12	89.34	$Na_2Ni(CN)_4 \cdot 3H_2O$
987.14	8.97	15.25	7.25	92.30	95.00	89.38	$Na_2Pt(CN)_4 \cdot 3H_2O$
1003.24	8.94	15.30	7.38	92.77	95.70	89.17	$Li_2Pd(CN)_4 \cdot 3H_2O$
1007.73	8.99	15.31	7.36	92.33	95.33	89.22	$Na_2Pd(CN)_4 \cdot 3H_2O$
1013.01	8.93	15.46	7.379	92.52	95.50	89.17	$K_2Ni(CN)_4 \cdot 3H_2O$
1023.06	8.99	15.40	7.43	92.37	95.48	89.62	$Rb_2Ni(CN)_4 \cdot 3H_2O$

[a] Data from references (*8*) and (*22*)

derived from the published data on $K_2Ni(SO_4)_2 \cdot 6H_2O$ (*19*) which should be a good approximation to $K_2Ni(SO_4)_{2-x}(SeO_4)_x \cdot 6H_2O$. Using the characteristic K-absorption edge of Se, Philip P. North determined the value of x as 0.60 ± 0.10. An approximate value of x can also be obtained from the fractional change in lattice constants for $(NH_4)_2Mg(SeO_4)_2 \cdot 6H_2O$ (*20*) and $(NH_4)_2Mg(SO_4)_2 \cdot 6H_2O$ (*21*); namely, $\Delta a/a$ = (9.42 kX − 9.28 kX)/9.42 kX = 0.0149, $\Delta b/b$ = (12.72 kX − 12.57 kX)/12.72 kX = 0.0118, and $\Delta c/c$ = (6.30 kX − 6.20 kX)/6.30 kX = 0.0159. The corresponding fractional changes for $K_2Ni(SO_4)_{2-x}(SeO_4)_x \cdot 6H_2O$ and $K_2Ni(SO_4)_2 \cdot 6H_2O$ are $\Delta a/a$ = 0.00685, $\Delta b/b$ = 0.00458, and $\Delta c/c$ = 0.00616. By linear interpolation, one obtains three values for x (0.92, 0.78, and 0.77) or a mean of 0.82 ± 0.10.

As in the case of the orthorhombic prototype charts, the utility of the monoclinic charts of Figure 2 may be extended to monoclinic phases with axial ratios falling within 0.465 and 0.770 and β within 104° to 110°. Usually one attempts to index only the first 5 to 10 largest d spacings and then proceeds to calculate provisional lattice constants for further numeric attempts at indexing the entire powder pattern.

TRICLINIC ISOMORPHS

Two innovations are introduced in the construction of the triclinic charts: first, the practice of plotting log d_{hkl} as a function of axial ratios is modified; and second, the drawing of the triclinic charts is performed by the IBM 1130 Data Presentation System. For the triclinic structure pertaining to $Na_2Ni(CN)_4 \cdot 3H_2O$ (*22*) (see Table V), the mean lattice constants are $\bar{a}$ = 8.913 Å, $\bar{b}$ = 15.23 Å, $\bar{c}$ = 7.330 Å, $\bar{\alpha}$ = 92.45°, $\bar{\beta}$ = 95.39°, and $\bar{\gamma}$ = 89.24°. Inasmuch as the respective angles for the 8 isomorphs of Table V are nearly constant, one proceeds by computing log d_{hkl} as a function of one of the cell edges of the reciprocal unit cell while holding the other lattice parameters constant at their respective mean values. Expression 3 gives the functional dependence of log d_{hkl}

$$\log d_{hkl} + \text{constant} = -\tfrac{1}{2}\log(h^2\rho_1^2 + k^2 + l^2\rho_2^2 + 2kl\rho_2\cos\alpha^* + 2lh\rho_1\rho_2\cos\beta^* + 2hk\rho_1\cos\gamma^*) \quad (3)$$

where $\rho_1 = d_{010}/d_{100}$, $\rho_2 = d_{010}/d_{001}$; and α^*, β^*, γ^* are the angles of the reciprocal cell. The log d_{hkl} values of all spacings greater than 2.500 Å were computed, arranged in descending order, and stored for subsequent automatic plotting by the IBM 1130 Data Presentation System. Thomas P. Blumer wrote the program to include the calculated relative intensity for each reflection (*22*, *23*) and the format for plotting two split strips on blank "strip chart" paper. Computation required 15 minutes; plotting, 40 minutes. Lettering was performed manually on the three graphs which were then spliced to produce Figure 3. The alignment of the six charts was set by the 020 reflection. Although 31 different split charts can be constructed for the triclinic system, one can reduce this number considerably for a particular structure because of the small variations of the respective lattice constants within an isomorphous series and because of the fortuitous constancy of two or more cell constants.

The main purpose of constructing the triclinic charts is to demonstrate the automatic plotting of the split charts and thus permit establishing an atlas of structure charts for the important, representative, biaxial crystals.

ACKNOWLEDGMENT

The author is grateful to the management of The Dow Chemical Company for granting him a sabbatical leave and he is equally appreciative of the courtesies extended to him by the Department of Chemistry of The Johns Hopkins University. To Thomas J. Kistenmacher, he is indebted for carefully reviewing the manuscript.

RECEIVED for review December 16, 1971. Accepted May 25, 1972.

(20) W. Hofmann, *Z. Kristallogr.*, **82**, 323 (1932).
(21) *Ibid.*, **78**, 279 (1931).
(22) H. Brasseur and A. de Rassenfosse, *Mém. Soc. Roy. Sci. Liège*, [2] **4**, 397 (1941).
(23) D. K. Smith, "A Fortran Program for Calculating X-ray Powder Patterns from the Atom Coordinates," American Crystallographic Association, Cambridge, Mass., March 28–30, 1963; paper E11.